

## Appendix A

# Theoretical treatments

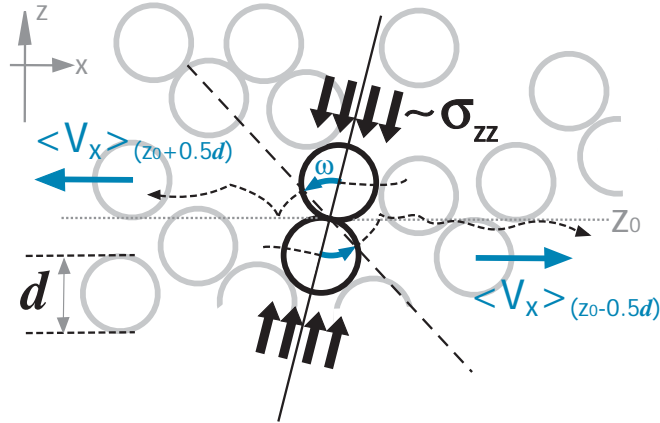


Figure A.1: Schematic representation of a granular shear flow. Two highlighted spheres are in contact at height  $z_0$ . The dashed curves represent the center-of-mass trajectories of each sphere.

## A.1 Criterion on stress and shear rate for creating a quasi-static granular flow

In this appendix, we derive a general criterion for the stress and shear rate for granular particles to be in a quasi-static regime. We use this criterion to estimate the upper bound of driving speeds for the sheared packing to be entirely in the state of quasi-static (creeping) flow, under our fixed normal load.

Consider uniformly sized, non-cohesive, rigid particles of mass  $m$  and diameter  $d$ , packed under a compressive load along  $z$  and sheared along  $+x$  and  $-x$ , as shown in Fig. A.1. Here we choose a local reference frame in which the value of time-averaged velocity  $\langle V_x \rangle$  as a function of height  $z$  appears anti-symmetric with respect to  $z_0$ , a reference height where the two highlighted particles contact. If the local granular stress is high enough to keep all contacting particles in either static or sliding contact for a finite duration (until they are eventually pulled apart), these two particles would move around the contact point with a radius of curvature  $d/2$  and an angular velocity  $\omega \approx \langle V_x \rangle_{z_0+0.5d} / 0.5d \equiv \dot{\gamma}$ . Because the assumed non-cohesive contacts between the two spheres only sustain a positive stress but not a tension, this is equivalent to the condition that the ‘normal’ component

( $F_N$ ) of the total force exerted by all surrounding particles on each of the two highlighted spheres needs to be greater than the centripetal force  $m\omega^2 d/2$  required for the local circular motion. That is,

$$m\dot{\gamma}^2 d/2 \approx m\omega^2 d/2 < F_N \approx \sigma_{zz} d^2 \quad (\text{A.1})$$

in which  $\sigma_{zz}$  stands for coarse-grained normal stress along the  $z$  direction. We can define a dimensionless number  $X \equiv \frac{1}{2}m\dot{\gamma}^2 d^{-1} \sigma_{zz}^{-1}$ , which represents <sup>1</sup> the ratio of the centripetal force per particle to the normal force per area  $d^2$ . The stress component  $\sigma_{zz}$  can either be mechanically imposed, or arise from grain's self-weight, or both. We can alternatively express  $\sigma_{zz} d^2$  as  $mgN_{eq}$ , in which  $N_{eq}$  is the equivalent number of layers whose weight produces a stress  $\sigma_{zz}$  at the location being considered. For granular materials in a sufficiently wide container where the Janssen effect can be neglected [38], grain weight contributes to the normal stress at any horizontal internal plane with the corresponding  $N_{eq}$  equal to the actual number of layers packed above the plane considered.

The shear rate  $\dot{\gamma}$  can be approximated by  $\frac{\langle V_x \rangle}{l}$  where  $l$  is the local exponential decay length for grain velocity. The empirical value of  $l$  is usually about a few particle diameters. For a packing sheared from above under the influence of gravity, the highest shear rate  $\dot{\gamma}$  and lowest stress  $\sigma_{zz}$  occur at the first layer adjacent to the shearing surface; therefore the criterion Eqn (A.1) becomes

$$m\left(\frac{U_0}{l}\right)^2 d/2 < \sigma_{zz} d^2 \quad (\text{A.2})$$

or alternatively

$$m\left(\frac{U_0}{l}\right)^2 d/2 < mgN_{eq} \quad (\text{A.3})$$

where  $U_0$  stands for the mean velocity of the first layer, which is close to the boundary speed. Using the parameters  $d = 10^{-1}\text{cm}$ ,  $N_{eq} = 10^2$ ,  $g = 10^3\text{cm/s}^2$  and an empirical value  $l = 3d$ , we estimate that the transition threshold for  $U_0$  is  $4 \times 10^3 d/\text{s}$ , which is more than two orders of magnitude higher than the highest driving speed  $12d/\text{s}$  used in our experiments. Therefore, the shear flows reported in this experimental work are entirely in the quasi-static (creeping) regime where  $X \ll 1$ .

---

<sup>1</sup>One can perhaps compare this dimensionless number with the Mach number defined in kinetic theories. With the substitutions  $v = \dot{\gamma}d$ ,  $P_0 = \sigma_{zz}$ ,  $\rho_0 \sim md^{-3}$ , and the definition (Mach number)  $\equiv v/(\gamma P_0/\rho_0)$ , one finds that  $X \sim (\text{Mach number})^2$ . (The  $\gamma$  here stands for the constant for adiabatic expansion  $D(P\rho^{-\gamma})/Dt = 0$ , with a value of  $\approx 1.4$  for air.)

When the shear rate  $\dot{\gamma}$  is high or the stress is low, it is possible to reverse Eqn (A.1) and the subsequent inequalities; for example, transition from the regime of creeping flow into the ‘granular gas’ regime can be found either locally or globally in high-speed annular shear cells [19, 25] with their normal load reduced by a counter-weight. For an inclined gravity-driven granular flow with an upper free surface, it is commonly observed that particles within a few grain diameters of the surface are in a dynamical regime that is qualitatively different from that of the creeping grains in the interior. (See the experiments and measured velocity profiles in Ref. [27, 50].) Note that with an upper free surface, the smallest meaningful value of  $N_{eq}$  in the estimate proposed here should be 1 instead of 0, due to the weight of the first layer itself.

In the preceding discussion, cohesivity, friction, finite rigidity (elasticity) of grains and their interaction with interstitial fluids are neglected; the analysis here is meant to be an order-of-magnitude estimate of the threshold above which the departure from creeping flow can occur.

## A.2 Velocity fields of ordinary fluid in a rectangular channel

In this appendix, we analyze the velocity field if the granular material in the channel is replaced with a fluid. The momentum balance for a continuous medium of density  $\rho$  is in general

$$\rho \frac{D}{Dt} v_i = \partial_j \{T_{ij}\} + \rho g_i \quad (\text{A.4})$$

where  $\frac{D}{Dt} \equiv (\frac{\partial}{\partial t} + \vec{v} \cdot \nabla)$  and  $\partial_j \equiv \frac{\partial}{\partial x_j}$ . For an *isotropic* fluid, the stress  $T_{ij}$  has the form

$$T_{ij} = -p \cdot \delta_{ij} + \eta(\partial_j v_i + \partial_i v_j) \quad (\text{A.5})$$

where  $p$  stands for pressure.<sup>2</sup> For a *Newtonian* fluid, the viscosity  $\eta$  is by definition a constant independent of the local velocity gradient of the fluid.

Assuming the fluid is *incompressible*, i.e.  $\nabla \cdot \vec{v} = 0$ , Eqn (A.4) reduces to

$$\rho \frac{D}{Dt} v_i = (\partial_j \eta)(\partial_j v_i + \partial_i v_j) + \eta \nabla^2 v_i - \partial_i p + \rho g_i \quad (\text{A.6})$$

which is in the form of the Navier-Stokes equation except for the additional non-Newtonian term  $(\partial_j \eta)(\partial_j v_i + \partial_i v_j)$ .

---

<sup>2</sup>For simplicity, the distinction between shear viscosity and extensional viscosity is ignored.

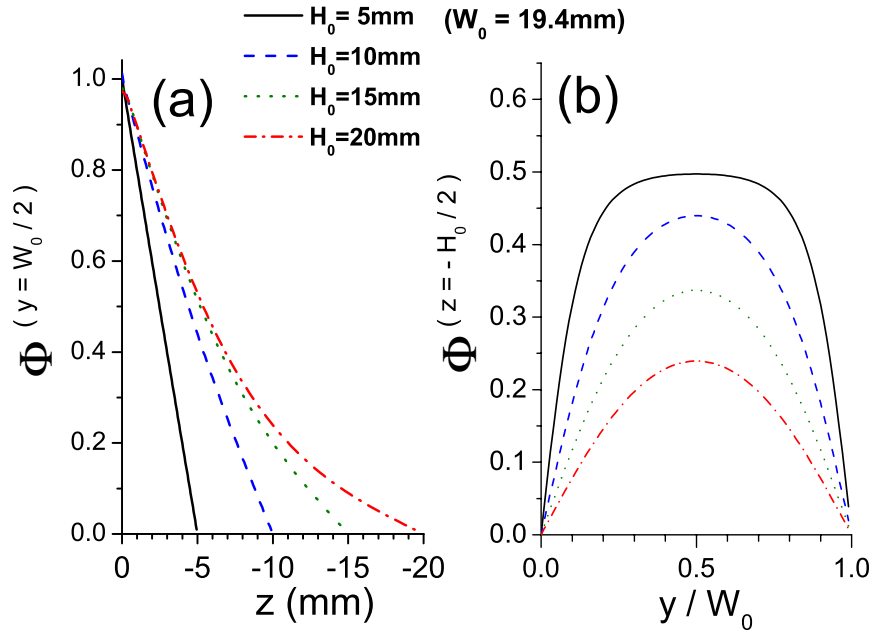


Figure A.2: The solution of Laplace equation  $\nabla_{yz}^2 \Phi = 0$  with no-slip boundary conditions:  $\Phi|_{z=0} = 1$  for the upper boundary,  $\Phi|_{y=0} = \Phi|_{y=W_0} = 0$  for the two vertical sidewalls, and  $\Phi|_{z=-H_0} = 0$  for the bottom. (a) Vertical profiles of  $\Phi$  at  $y = W_0/2$  as functions of  $z$ , for different values of  $H_0$ . The curves approach a linear profile when the aspect ratio  $\frac{H_0}{W_0}$  is small, and an exponential profile when  $\frac{H_0}{W_0}$  is large. (b) Horizontal profiles of  $\Phi$  at the mid-height  $z = -H_0/2$  as functions of  $y$ , for different values of  $H_0$ .

Assuming the stationary solution has the form  $\vec{v} = \Phi(y, z)\hat{e}_x$  with the gravity  $\vec{g}$  being parallel to the  $z$  axis, Eqn (A.6) reduces to

$$0 = (\nabla_{yz}\eta) \cdot (\nabla_{yz}\Phi) + \eta\nabla_{yz}^2\Phi \quad (\text{A.7})$$

In the simplest case of a Newtonian fluid where  $\eta$  is a constant, the problem reduces to Laplace equation  $\nabla_{yz}^2\Phi = 0$ . By specifying boundary conditions  $\Phi|_{y=0} = \Phi|_{y=W_0} = 0$  for the two vertical sidewalls,  $\Phi|_{z=-H_0} = 0$  for the bottom, and a flat profile  $\Phi|_{z=0} = 1$  at the upper surface, the solution is

$$\Phi(y, z) = \sum_n^{\text{Odd}} \frac{4}{n\pi} \left( \frac{\sinh \lambda_n z}{\tanh \lambda_n H_0} + \cosh \lambda_n z \right) \sin \frac{n\pi y}{W_0} \quad (\text{A.8})$$

in which  $\lambda_n \equiv n\pi/W_0$ . The principal (longest) decay length in this case is  $\lambda_1^{-1} = W_0/\pi$ , which is also reflected by the approximate slope of the curves shown in the semi-log plot Fig. 5.5. Samples of vertical and horizontal profiles of Eqn (A.8) for our channel with a fixed width  $W_0$ , at different packing thickness  $H_0$ , are demonstrated in Fig. A.2.

Note that, more generally, if one specifies an arbitrary velocity profile at  $z = 0$  with no-slip conditions on the other three stationary boundaries, the principal decay length will be selected by the lowest non-vanishing wave number along  $y$  as  $\Phi|_{z=0}$  is decomposed into sinusoidal components. That is, the principal length is determined by the spatial symmetry of the speed profile at  $z = 0$ .

### A.3 Derivation of Eqn (5.7)

By introducing a velocity-dependent sidewall friction Eqn (5.6) and assuming  $v^{slip}(z) = V_x(z)$ , the stress balance Eqn (5.2) yields a differential-integral equation

$$\ln[V'_x(z)/V'_x(0)] = \frac{1}{L_\alpha} \int_0^z (1 + \beta \ln[V_x(z')/V_x(0)]) dz' \quad (\text{A.9})$$

in which  $L_\alpha \equiv (\frac{2\sigma_0^W}{\alpha\sigma_0 W_0})^{-1}$ . This mathematical problem can be defined alternatively in terms of the local decay rate  $\lambda(z) \equiv V'_x(z)/V_x(z)$ . Using the identity  $V'_x(z) = \lambda(z)V_x(z) = \lambda(z)V_x(0) \exp \int_0^z \lambda(z') dz'$ , Eqn (A.9) can be rewritten as

$$\ln[\lambda(z)/\lambda(0)] + \int_0^z \lambda(z') dz' = \frac{1}{L_\alpha} \int_0^z (1 + \beta \int_0^{z'} \lambda(z'') dz'') dz' \quad (\text{A.10})$$

and  $V_x(z)$  can be obtained after  $\lambda(z)$  is determined. Differentiating Eqn (A.10) gives

$$\lambda(z) = -\frac{\lambda'(z)}{\lambda(z)} + \frac{1}{L_\alpha} \left(1 + \beta \int_0^z \lambda(z'') dz''\right) \quad (\text{A.11})$$

which is a differential-integral equation of  $\lambda(z)$ .

In order to find approximate solutions to Eqn (A.10), we use this equation to define an iteration. We denote the  $n$ -th iteration as  $\lambda^{(n)}(z)$  and assign  $\lambda^{(0)}(z)$  to be a constant. First of all,

$$\lambda^{(0)}(z) = \frac{1}{L_\alpha} \quad (\text{A.12})$$

is required by the self-consistency at  $z = 0$ . Iterating Eqn (A.10) gives

$$\lambda^{(1)}(z) = \frac{1}{L_\alpha} \left(1 + \frac{\beta}{L_\alpha} z\right) \quad (\text{A.13})$$

$$\lambda^{(2)}(z) = -\frac{\frac{\beta}{L_\alpha}}{1 + \frac{\beta}{L_\alpha} z} + \frac{1}{L_\alpha} \left(1 + \frac{\beta}{L_\alpha} \left(z + \frac{\beta}{L_\alpha} \frac{z^2}{2}\right)\right) \quad (\text{A.14})$$

and successively higher order terms of  $\frac{\beta}{L_\alpha}$ .

By integrating the first approximation Eqn (A.13), we obtain

$$\ln[V_x(z)/V_x(0)] = \frac{1}{L_\alpha} \cdot \left(z + \frac{\beta}{2L_\alpha} z^2\right) \quad (\text{A.15})$$

which has the form of a quadratic function that satisfactorily fits the experimental data described in Fig. 5.4.

It should be pointed out that neither the iteration procedure is unique, nor the iteration is the only method to approximate the solution. The convergence and effectiveness of different approximation schemes that can be used to solve Eqn (A.10) need further investigation. Any useful approximation scheme or numerical solution may require a validity interval in  $z$  that is several times wide the assumed value of  $L_\alpha$ .